Wearable Inertial Sensor-Based Limb Lameness Detection and Pose Estimation for Horses

Tarik Yigit, *Graduate Student Member, IEEE*, Feng Han, *Graduate Student Member, IEEE*, Ellen Rankins, Jingang Yi, *Senior Member, IEEE*, Kenneth H. McKeever, and Karyn Malinowski

***Abstract*— Accurate objective, automated limb lameness detection and pose estimation play an important role for animal well-being and precision livestock farming. We present a wearable sensor-based limb lameness detection and pose estimation for horse walk and trot locomotion. The gait event and lameness detection are first built on a recurrent neural network (RNN) with long short-term memory (LSTM) cells. Its outcomes are used in the limb pose estimation. A learned low-dimensional motion manifold is parameterized by a phase variable with a Gaussian process dynamic model. We compare the RNN-LSTM-based lameness detection method with a feature-based multi-layer classifier (MLC) and a multi-class classifier (MCC) that are built on support vector machine/K-nearest-neighbors and deep convolutional neural network methods, respectively. Experimental results show that using only accelerometer measurements, the RNN-LSTM-based approach achieves 95% lameness detection accuracy and also outperforms the feature-based MLC or MCC in terms of several assessment criteria. The pose estimation scheme can predict the 24 limb joint angles in the sagittal plane with average errors less than 5 and 10 degs under normal and induced lameness conditions, respectively. The presented work demonstrate the successful use of machine learning techniques for high performance lameness detection and pose estimation in equine science.**

***Note to Practitioners*—Automation technologies are increasingly used for precision agriculture but few have focused on monitoring individual animals in open field for precision livestock farming. Limb lameness detection and pose estimation in open field is labor-intensive, unsafe for farmers, and inefficient. The presented machine learning-enabled, wearable inertial sensor-based design provides an effective and efficient approach for horse limb lameness detection and pose estimation applications. We present an RNN-LSTM for lameness detection and an integrated manifold learning model is used to predict the horse limb joint angles in walk and trot gaits under normal and induced lameness conditions. We also present a systematic analysis and experiments to demonstrate the impacts of the wearable sensor locations and signal information on lameness detection and pose estimation performance. Several other machine learning-based lameness detection methods are also presented and compared. The extensive multi-horse testing results are presented to demonstrate the superior accuracy and higher performance than other types of machine learning methods. One attractive feature of the proposed design lies in its high performance and fast computational capability for potential real-time applications in open field.**

***Index Terms*— Equine gait analysis, lameness detection, inertial measurement units, pose estimation, machine learning.**

Manuscript received 26 October 2021; revised 27 January 2022; accepted 25 February 2022. Date of publication 28 March 2022; date of current version 5 July 2022. This article was recommended for publication by Associate Editor W. Shen and Editor M. Dotoli upon evaluation of the reviewers' comments. The work of Jingang Yi was supported in part by the U.S. National Science Foundation under Award CMMI-1762556 and Award CNS-1932370. The work of Kenneth H. McKeever was supported by the Rutgers Equine Science Center and the New Jersey Agricultural Experiment Station. An earlier version of this paper was presented in part at the 2020 IEEE International Conference on Automation Science and Engineering (Virtual Conference) in August 2020. *(Tarik Yigit and Feng Han contributed equally to this work.) (Corresponding author: Jingang Yi.)*

This work involved human subjects or animals in its research. Approval of all ethical and experimental procedures and protocols was granted by the Rutgers University Institutional Animal Care and Use Committee (IACUC) under Protocol No. PROTO999900214.

Tarik Yigit, Feng Han, and Jingang Yi are with the Department of Mechanical and Aerospace Engineering, Rutgers University, Piscataway, NJ 08854 USA (e-mail: ty127@scarletmail.rutgers.edu; fh233@scarletmail.rutgers.edu; jgyi@rutgers.edu).

Ellen Rankins, Kenneth H. McKeever, and Karyn Malinowski are with the Equine Science Center, Rutgers University, New Brunswick, NJ 08901 USA (e-mail: emr219@sebs.rutgers.edu; mckeever@sebs.rutgers.edu; karynmal@njaes.rutgers.edu).

Color versions of one or more figures in this article are available at https://doi.org/10.1109/TASE.2022.3157793.

Digital Object Identifier 10.1109/TASE.2022.3157793

I. Introduction

ANIMAL diseases are responsible for an average loss of more than 20% of animal production worldwide and economic and societal impacts are significant [1]. Lameness is considered as a symptom of underlying pathological afflictions [2], [3]. Animals with lameness often demonstrate a deviation of the normal gait, i.e., abnormal gait. It is reported that only in the USA, the economic cost for equine lameness has been estimated ranging from USD $678 million to $1 billion in 1998 [4]. Real-time, holistic evaluation and gait analysis are effective ways to reliably identify and predict early-stage lameness or disease infection to improve animal well-being and enable proactive interventions for animal production loss [5].

Detecting lameness is a labor intensive, expensive and challenging task for veterinarians [6]. Most of the lameness evaluation is built on visual examinations and relies on the observations of movement asymmetries [7]. A great gap exists between the levels of awareness of lameness by different observers and therefore, the evaluation results are subjective depending on examiner's personal and technical experience [8]. Using locomotion data collected by wearable sensors and applying statistical analysis with specific features is a trend in lameness study [9]. The common sensors used include optical motion capture systems and force plates [10]. The high cost and indoor usage of cameras and force plates restrict wide applications in farming industry. Wearable inertial

measurement units (IMUs) have been commonly used to collect large livestock motion data for gait analysis and lameness detection due to their small-size, light-weight, low-cost and setup convenience [11]–[13]. For large livestock such as horse, small-size IMUs are attached to the limbs and body and provide non-intrusive motion measurements without causing gait changes.

Although various accurate, field-deployable sensing technologies have been reported for enabling real-time monitoring of animals [9], [14], few are focused on limb pose (i.e., joint angle) estimation. Motion capture or machine vision systems are the main sensing modality to obtain the animal gaits and poses. In [15], [16], horse forelimb and hindlimb joint angles are presented for trot gait using motion capture systems. The limb kinematics and ground reaction forces for horse walk are obtained by video analysis and force plates, respectively in [17], [18]. The motion capture or machine vision systems are expensive and also difficult for use in open field and outdoor environment. Wearable IMUs were used in recent years for real-time human pose estimations [19]–[24]. Particularly, the work in [20] used wearable IMUs to estimate the lower-limb joint angles for equestrian sports riders and the study does not include horse limb pose estimation. Indeed, few research has been reported for wearable IMU-based joint angles estimation for horses or quadrupedal animals.

Most of the IMU-based gait analysis use statistical approaches to investigate particular bio-features to assess horse lameness. These features include withers and pelvis movement asymmetries, proximal flexion tests of hindlimbs and horizontal velocity and acceleration of forelimbs on hoof-off and hoof-on events, and the stride duration [25]–[27], etc. Although successful evaluation results were reported [28], [29], these approaches only consider particular features and lack comprehensive analysis of locomotion. This motivates us to use machine learning techniques to generate a holistic approach for lameness detection from all limb IMUs. It is also of interest to analyze and identify the wearable sensor locations and selective signal (i.e., acceleration or angular rate) contributions to limb lameness detection and pose estimation.

Emerging techniques such as machine learning provide promising approaches for IMU-based bipedal gait detection and pose estimation [22], [30]. The number of used wearable IMUs and their locations on human body for the best gait estimation performance were reported (e.g., [31], [32]). Unlike bipedal locomotion, the quadrupedal gaits of large-size animals such as horses are much more complex in terms of the gait styles and the number of joint angles [33], [34]. In recent years, machine learning methods were increasingly used for animal gait analysis and lameness detection. Decision tree induction was applied for animal lameness detection and claimed to be useful with small data-sets [35]. A two-phase classifier has been developed for sheep lameness detection in [36]. In [37], a long-short term memory (LSTM) network was used to accurately identify horse gaits using seven wearable IMUs on the body and limbs. Similarly, five different machine learning models including support-vector machine (SVM), Gaussian process regression GPR, decision tree, boosted trees and random forest were used to predict horse velocity using seven body-mounted IMUs. However, these studies do not use wearable sensors to estimate the limb joint angles and the machine learning techniques have not been reported for applications such as horse lameness detection.

In this paper, we present a machine learning-based limb lameness detection and pose estimation scheme for horse trot and walk. The pose estimation and lameness detection design is built on the acceleration and gyroscope measurements from four IMUs that are attached to four limbs each. A recurrent neural network (RNN) with LSTM cells is used to detect the gait and induced lameness on forelimb during trot and walk. The gait and lameness detection only uses accelerometer measurements. A manifold learning method is taken to predict limb joint angles with the gyroscope measurements. Inspired by the work in [38] for human upper-limb joint angle estimation, we use a Gaussian process dynamic model (GPDM) to construct the horse limb motion manifold. A phase variable is used to parameterize the GPDM for real-time joint angles estimation. We also compare the lameness detection results with the feature-based multi-layer classification (MLC) that was reported previously in [39] and a multi-class classifier such as deep convolutional neural network (DCNN) [40]. The MLC includes gait classification, limb lameness detection, and lameness localization layers by considering the property of horses motion and is built on the SVM and K-nearest-neighbors (KNN) methods. The experimental results confirm the effectiveness and efficacy of the proposed detection and evaluation scheme. We also discuss and analyze the signal selection (i.e., gyroscope and accelerometer) of the limb IMUs for lameness detection and pose estimation.

The main contributions of the work are two-folds. First, using machine learning (i.e., RNN-LSTM) for horse lameness detection is new. To the author's best knowledge, no similar work has been reported for horse lameness detection. Comparing with other horse lameness detection methods that rely mainly on specific asymmetric features, the proposed RNN-LSTM method provides an automated, holistic features selection from all wearable limb IMUs. One additional attractive feature for RNN-LSTM design is the real-time capability for lameness detection and pose estimation. Second, the proposed limb joint angle estimation for animal locomotion is novel. Although the similar approaches are used for human walk, the GPDM-enabled pose estimation is the first reported result for quadrupedal locomotion. The proposed lameness and pose estimation method provides an effective enabling tool for field deployment for future precision livestock farming. The work in this paper significantly extends the MLC that was reported in previous conference publication [39] with the new RNN-LSTM-based lameness detection and the GPDM-based pose estimation design and many additional analyses and experiments.

The rest of this paper is organized as follows. Data collection and problem statement are discussed in Section II. Section III presents the RNN-LSTM and MLC approaches for gait activity and lameness detection. We discuss the GPDM-based limb pose estimation in Section IV and the performance evaluation metrics in Section V. The experimental

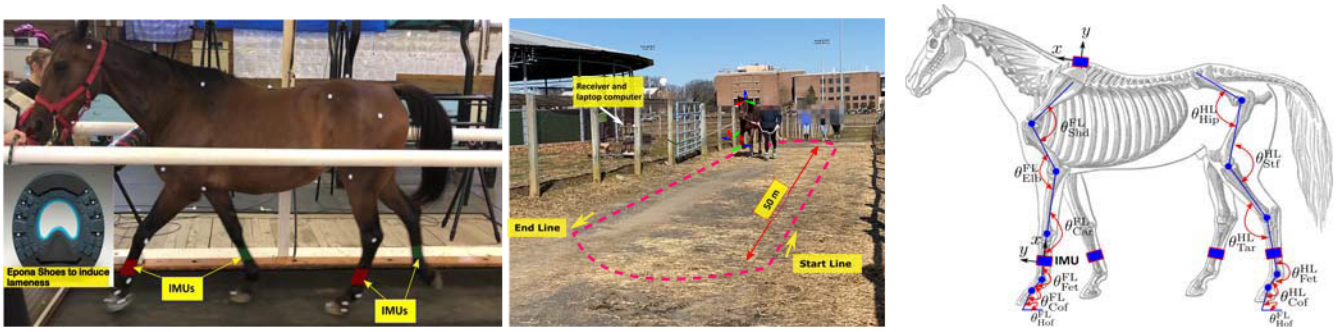

(a) (b) (c)

Fig. 1. (a) Indoor horse gait and locomotion data collection setup on a treadmill. A motion capture system and wearable IMUs are used in experiments. A plastic shoe is attached to fore hoof to introduce gait changes (i.e., induced lameness) in both indoor and outdoor experiments. (b) Outdoor horse locomotion experiments using a 50-m runway. Plastic shoes are used and attached to horse forelimbs to induce gait alterations in data collection. (c) Schematic of the forelimb and hindlimb joint angles and IMU locations.

results are presented in Section VI before we summarize the concluding remarks in Section VIII.

II. Horse Locomotion Experiments and Problem Statement

A. Experiments and Data Collection

Experimental data were collected at the Equine Exercise Physiology Laboratory at Rutgers University. Both indoor and outdoor horse locomotion experiments were conducted. Fig. 1(a) shows the indoor experimental setup on a treadmill and Fig. 1(b) illustrates the outdoor experiment with wearable IMUs. Four wearable IMUs are attached and firmly secured on the lateral portion of the distal third metacarpal and third metatarsal with self-adhesive bandages with one on each limb. The x-axis of the limb IMUs was oriented along the vertical axis and z-axis was oriented along the frontal axis. The y-axis was oriented along the sagittal axis with the positive axes oriented cranially on the left and caudally on the right; see Fig. 1(c). Another IMU was attached at the withers location. The lameness detection and pose estimation algorithms do not use the fifth IMU at the withers but it is used only for comparison purpose. The IMUs were attached to the horse limbs by equine science professionals to minimize the possible intrusive effect. Before the actual IMU data were recorded and collected, a few warm-up trails were conducted to allow the horses to adapt to the wearable sensors.

For indoor experiments, each limb IMU (from INSENCO Inc., Hangzhou, China) included a triaxial accelerometer and a triaxial gyroscope. The ranges of accelerometer and gyroscope are $\pm 100\,g$ ($g = 9.8$ m/s^2 is the gravitational constant) and ± 4000 deg/s, respectively. The IMU measurements were sampled and collected at a frequency of 100 Hz. An optical motion capture system (8 Bonita cameras, Vicon, Inc., Oxford Metrics, Oxford, UK) was used to capture the limb motion. Following the recommendations in [41], a total of 37 retroreflective markers were placed on the horses. Eight markers were placed on the lateral side of the left and right forelimb each to evaluate angles between the proximal and distal segments of the joints: the proximal end of the spine of the scapula, shoulder joint, elbow joint, carpal joint, fore fetlock joint, coffin joint, fore hoof and fore toe. Another eight markers were placed on the lateral side of the left and right hindlimb each: the ventral aspect of the tuber coxae (point of the hip), hip joint, stifle joint, talus (hock joint), hind fetlock joint, coffin joint, hind hoof, and hind toe. Five additional markers were mounted on the back along the vertebral column at the withers, lumbar-sacral junction, point of the croup, and on the right and left side of the temporal bone, along the zygomatic process. For walk and trot, the treadmill speeds were controlled around 1.62 m/s and 4.18 m/s, respectively. For outdoor experiments, horses were instrumented with four IMUs (MPU-9250 from Noraxon, Scottsdale, Arizona, USA) [42]. The ranges of accelerometer and gyroscope are $\pm 16\,g$ and ± 2000 deg/s, respectively. The IMU measurement data were wirelessly transmitted to the receiver and displayed on a laptop at a frequency of 400 Hz; see Fig. 1(b).

TABLE I
Basic Information About Horses in Experiments

SN	Height at withers (cm)	Gender	Age	Shoeing
1	154.3	Gelding	13	Barefoot
2	154.9	Gelding	13	Barefoot
3	153	Mare	5	Barefoot
4	160	Mare	15	Barefoot
5	149.9	Mare	16	Shod/Hind hooves only
6	156.8	Mare	17	Barefoot

Experimental data were collected from six horses (Standardbreds). Table I lists the detailed information about the horses. Two plastic shoes (from EponaMind, Paso Robles, California, USA) as shown in Fig. 1(a) were attached to the left or right fore hoof in a randomized order to induce gait alterations or lameness. The induced lameness (abnormal gait) was used to evaluate the proposed lameness detection and pose estimation design. In each data collection session, horses completed twenty-four trials at walk and trot each under three conditions: controlled normal gaits, shoe on left front, and shoe on right front. For outdoor experiments, one trial consists of the horse being led by a handler at the appropriate gait along a straight 50-m runway as shown in Fig. 1(b). Between two trials horses turned around to traverse back over the runway and the process repeated until twenty-four trials were completed. The data collection resulted in six distinct classes of data: normal

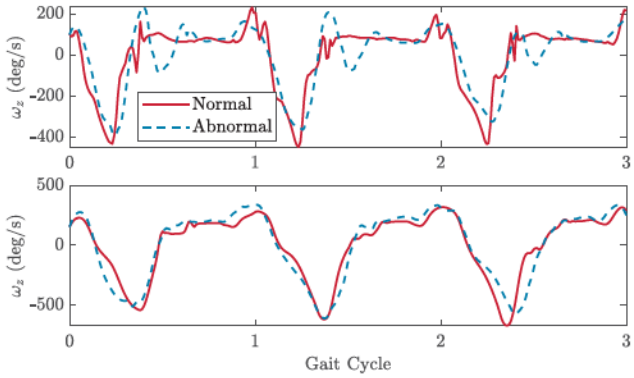

Fig. 2. Raw IMU (on left forelimb) gyroscope measurements about the z-axis under the normal and abnormal conditions for the horses walk (top) and trot (bottom) gaits.

walk, normal trot, walk with shoe on left or right fore hoofs, and trot with shoe on left or right fore hoofs. The testing protocol was approved by the Institutional Animal Care and Use Committee (IACUC) at Rutgers University.

We obtain and extract the gait cycle and limb pose information from the motion capture system and the wearable limb IMU data. For joint angle estimation, this work mainly focuses on forelimb and hindlimb joint angles in the sagittal plane. Fig. 1(c) illustrates these joint angles. We denote θ^{Fi}_{Hof} θ^{Fi}_{Cof}, θ^{Fi}_{Fet}, θ^{Fi}_{Car}, θ^{Fi}_{Elb}, and θ^{Fi}_{Shd}, $i = L, R$, for the hoof, coffin, fetlock, carpus, elbow and shoulder joint angles for the left and right forelimb, respectively. Similarly, θ^{Hi}_{Hof},θ^{Hi}_{Cof}, θ^{Hi}_{Fet}, θ^{Hi}_{Tar}, θ^{Hi}_{Sti}, and θ^{Hi}_{Hip}, $i = L, R$, are used to denote the hoof, coffin, fetlock, tarsus, stifle and hip joint angles for the left and right hindlimb, respectively. Only the hoof joint angles are absolute and all others are relative joint angles [18], [43]. To calculate and evaluate these joint angles, we first form the sagittal plane using the marker on the point of the croup, medial midpoints of the markers on the hip joints, and the points of the hip. Then, all other markers' positions are projected on the sagittal plane by an orthogonal projection. Link vectors for the proximal and distal segments for each limb are calculated using the projected markers' positions on the sagittal plane and finally the joint angles are computed by the relative angles between two adjacent corresponding link vectors.

For walk and trot, each limb touches down on the ground and then swings periodically and both are symmetric gaits, i.e., each limb repeats similar pattern for stance and swing phases. To capture the periodic steady-state walk and trot gait, we use phase variable, denoted by $s \in [0, 1]$, as the normalized gait progression by each cycle duration (between two consecutive hoof touchdowns). Different approaches exist in the literature to extract gait cycle events, that is, to determine hoof-on and hoof-off events. It has been observed that acceleration rises sharply from a negative peak to a positive peak when the hoof contacts the ground [11]. To construct the feature-based MLC algorithm, we create gait cycle routines by stacking three linear acceleration and three gyroscope measurements (total 6 signals) from four IMUs into a signal array of size $24 \times N_s$, where N_s is the number of samples within one gait cycle. As an example, Fig. 2 shows the raw IMU gyroscope measurements about the z-axis (i.e., the transversal axis of

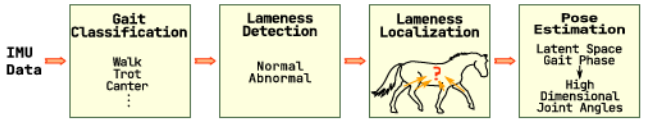

Fig. 3. Schematic of the multi-layer lameness detection classification and pose estimation.

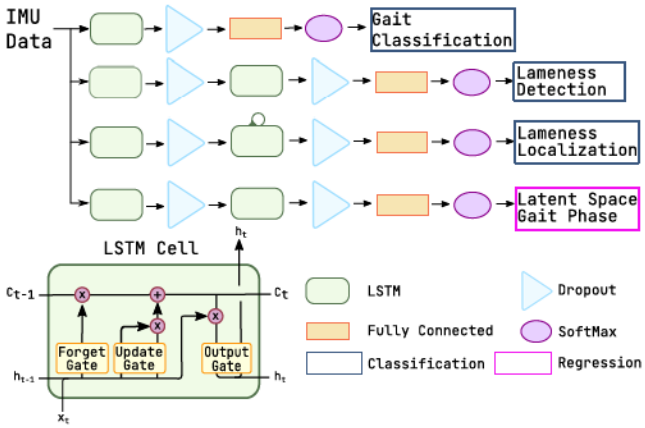

Fig. 4. Schematic of the lameness detection and gait phase estimation by LSTM.

the major rotation of the metacarpal bone) under normal and abnormal walking and troting on the indoor treadmill.

B. Problem Statement

The problem statement of this work is to design a limb lameness detection and poses (i.e., joint angles) estimation scheme for horse walk and trot under normal and induced abnormal conditions using the complete or partial measurements from four wearable limb IMUs. It is desirable to have the design for real-time, open field applications.

III. Limb Lameness Detection

In this section, we first discuss an overview design for limb lameness and gait activity detection. We then present an RNN-LSTM and a feature-based MLC implementation.

A. Overview

The gait and lameness detection scheme is built on a layer-by-layer approach to identify the property of current data and detect the lameness occurrence and location step-by-step. The scheme provides the flexibility of using different classification algorithms at each layer. Fig. 3 illustrates the schematic of the multi-layer lameness detection and pose estimation approach. We consider and assign three properties associated with each motion data instance: gait, lameness situation, and lameness location. For example, for walk and trot with induced lameness at horse forelimb, the data are accordingly categorized into six groups: normal walk (NW), normal trot (NT), abnormal walk with left or right forelimb lameness (denoted as LW or RW), and abnormal trot with left or right forelimb lameness (denoted as LT or RT).

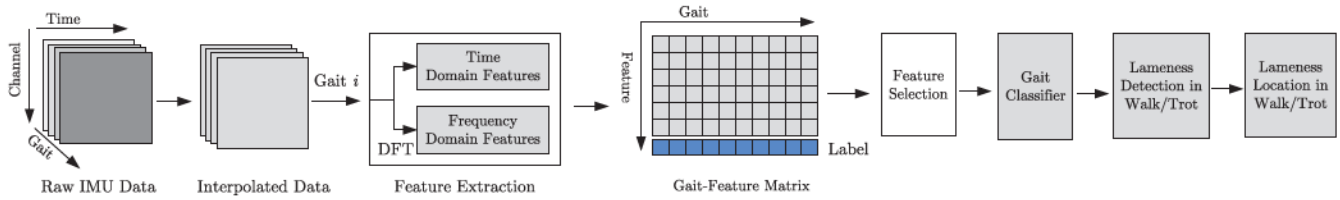

Fig. 5. The structure of feature extraction based multi-layer classifier for horse lameness detection.

Instead of recognizing the data with one label (e.g., left forelimb lameness walk) that contains the above three properties, we consider to use three labels (e.g., left forelimb, lameness, and walk) that each corresponds to one property. By doing so, we identify the property of the data layer-by-layer and therefore, the multi-class problem is transferred to a multi-layer classification problem. In each layer, the data are compared in terms of one single property. As shown in Fig. 3, three layers are constructed: the gait classifier (GC) (top layer), lameness detection within walk (LDW) or trot (LDT) (middle layer), and lameness localization within walk (LLW) or trot (LLT) (bottom layer). Additional advantages of using multi-layer classifiers include reducing the class of current layer and possibly forming a binary classification, reducing the cost of time and storage for training and testing data, and providing quantitative methods for horse lameness evaluation and flexibility to design each classifier independently. The last module in Fig. 3 is for pose estimation that will be discussed in the next section.

Using the above multi-layer structure, two different machine learning classifiers are used in implementation. The first one is the RNN-LSTM that uses the (partial) IMU measurements for classification. The second approach first extracts features from the IMU data and then feeds into the classifier at each layer.

B. Lameness Detection by RNN-LSTM

Lameness detection by the RNN-LSTM design directly uses the IMU measurement as input sequence. Fig. 4 illustrates overall network architecture for gait and lameness detection. Each LSTM cell (shown in the left bottom in the figure) includes a forget, an update and an output gate consecutively. When new information arrives, the cell first decides what to keep or forget in the current cell state, then determines what new information is stored and updates the cell state in order to finally filter out an output [44]. The LSTM architecture is highly efficient and the classifier can be used in real-time applications. To improve classification performance, multiple LSTM layers are added to construct a deep neural network.

For walk and trot with induced lameness in forelimb, we separately train five classifiers: one for GC, two for LDW and LDT, and two for LLW and LLT as described above. As shown in Fig. 4, gait classification in the first layer uses a single LSTM cell with 100 hidden units. It is followed by a `Dropout` (0.2) layer to randomly drop 20% units from the network to prevent overfitting of the model. The outputs from the dropout layer are passed through a fully connected layer with `ReLU`. Finally, the classification is done based on the probability outputs from the `Softmax` activation function, which converts the class scores to probabilities such that the gait with the highest probability is detected. Two classifiers in the lameness detection and localization layers include an additional LSTM cell with 120 hidden units and another `Dropout` (20%) module in front of the LSTM with 100 units.

The IMU data in each stride are considered as one data point. In particular, since the horse motion is not exactly periodical, each data point has different duration. The LSTM-based classifier does not require to normalize each stride into the same size and using the same configuration, different combinations of the IMU data can be fed into the classifier to identify the most sensitive channels in the IMU measurements for normal and abnormal conditions.

C. Feature-Based MLC Lameness Detection

The MLC data feature is constructed in both time and frequency domains to provide comprehensive information. Only the sensitive components in data are then selected to train the classifier by feature selection algorithms by their importance. Fig. 5 illustrates the feature-based MLC lameness detection scheme. Before training the classification model, feature vectors from IMU data are extracted to form a single gait feature matrix (GFM) in both time and frequency domains.

1) Time Domain Feature: In time domain, we consider statistical measurements of the gait data. For each gait cycle data, the features include: (1) maximum, minimum, mean and standard deviation values of the each IMU signal channel; (2) quartiles data, including 25%, 50%, and 75% are the value that splits off the lowest 25%, median and highest 25% of the data, respectively; (3) skewness $S = \frac{1}{N_s\sigma^3}\sum_{i=1}^{N_s}(x_i - \bar{x})^3$ to describe the distribution of the data, where $\bar{x}$ and σ are the average and standard deviation of IMU data series $\{x_i\}_{i=1}^{N_s}$ for each gait cycle; and (4) singular value set of the magnitude matrix of acceleration and gyroscope measurements of each IMU unit, i.e., $\boldsymbol{\Sigma} = \sigma(\boldsymbol{M})$, where $\sigma(\cdot)$ represents the singular value operator, matrix $\boldsymbol{M} = [\boldsymbol{A}_1\ \boldsymbol{A}_2\ \boldsymbol{A}_3\ \boldsymbol{A}_4]$, $\boldsymbol{A}_i = [\|\boldsymbol{a}_i\|\ \|\boldsymbol{\omega}_i\|]^T$, and $\boldsymbol{a}_i, \boldsymbol{\omega}_i \in \mathbb{R}^3$ are the accelerometer and gyroscope measurement vectors of ith IMU, respectively, $i = 1, 2, 3, 4$.

2) Frequency Domain Feature: We apply the discrete Fourier transformation (DFT) to each channel of the IMU measurements to obtain the properties in frequency domain. The frequency domain features include: (1) ω_{max}: the frequency with maximum power, also known as dominant frequency; (2) harmonic frequency, i.e., frequencies with the second and third highest powers; and (3) harmonic ratio, which is the ratio of the sum of the even and odd frequency amplitudes.

The above selected time and frequency domains features also incorporate many commonly used characteristics for lameness detection, such as time duration of each gait and the

duration from the minimal value to the maximal value [36], etc. Using the above procedure, we convert all the gait cycles into feature vectors to form the GFM; see Fig. 5. Since the feature vector consists of many components, to avoid overfitting and decrease expense in the simulation, we select key components that are relevant to current classification problem intentionally. Feature selection also helps reduce the cost of time and storage for training and testing. For each classifier we select the top relevant components that are not necessarily the same in terms of size and content.

Classification algorithms used in the feature-based MLC includes the SVM method for GC (top layer) and the KNN method for LDW/LDT (middle layer) and LLW/LLT (bottom layer). Those two algorithms have been successfully used to detect the motion type and lameness of sheep [36]. The input are the features extracted from the IMU motion data and the ground truth labels. For KNN algorithms, the number of the neighbor is set as 10 and the Euclidean distance metric is used.

IV. GPDM-Based Limb Poses Estimation

In this section, the manifold learning method is adopted to estimate the 24 limb joint angles θ_j^i, i = FL, FR, HL, HR, j = Shd/Tip, Elb/Sti, Car/Tar, Fet, Cof, Hof, for a given gait activity. The high dimensional horse joint angles data are first processed through the GPDM to learn and obtain the low-dimensional dynamic latent model. By parameterizing the latent manifold dynamics with the gait phase variable, we are able to predict the horse pose through IMU measurements. For this work, we focus on horse walk and trot under normal and abnormal (limb lameness) conditions and therefore, a total of six gait activities such as NW, NT, LW, RW, LT and RT (defined in Section III-A) are considered.

For the ith gait activity, i = NW, NT, LW, RW, LT, RT, denoting $\boldsymbol{\theta} \in \mathbb{R}^D$ as the joint angles vector, where D is the joint angle dimension, the dynamics for latent variable $\boldsymbol{x} \in \mathbb{R}^d$ and observation mapping between $\boldsymbol{\theta}$ and $\boldsymbol{x}$ are obtained as manifold $\mathcal{M}_i$ as

$$\mathcal{M}_i : \begin{cases} \frac{d\boldsymbol{x}}{ds} = \boldsymbol{f}(\boldsymbol{x}, \boldsymbol{\alpha}) + \boldsymbol{n}_x \\ \boldsymbol{\theta} = \boldsymbol{g}(\boldsymbol{x}, \boldsymbol{\beta}) + \boldsymbol{n}_\theta, \end{cases} \tag{1}$$

where s is the gait phase variable, d is the latent space dimension, nonlinear functions $\boldsymbol{f}(\cdot,\cdot)$ and $\boldsymbol{g}(\cdot,\cdot)$ represent the latent dynamics vector field and the mapping from the latent space to the joint angle space, respectively. Variables $\boldsymbol{n}_x$ and $\boldsymbol{n}_\theta$ are zero-mean, white Gaussian noises, and $\boldsymbol{\alpha}$ and $\boldsymbol{\beta}$ are the hyperparameters for the latent dynamics and output observation functions.

In the GPDM framework, functions $\boldsymbol{f}$ and $\boldsymbol{g}$ are marginalized out by using the kernel-based method. We try to identify the optimal hyperparameters in the model by considering a Gaussian process (GP) for kernel function. Given joint angle data set $\boldsymbol{\Theta} = \{\boldsymbol{\theta}_i\}_{i=1}^N$, where N is the number of data points, and denoting $\boldsymbol{X} = \{\boldsymbol{x}_i\}_{i=1}^N$, the GPDM is indeed to maximize the following posterior probability

$$p(\boldsymbol{X}, \boldsymbol{\alpha}, \boldsymbol{\beta}|\boldsymbol{\Theta}) \propto p(\boldsymbol{\Theta}|\boldsymbol{X}, \boldsymbol{\beta}, \boldsymbol{W}) p(\boldsymbol{X}|\boldsymbol{\alpha}) p(\boldsymbol{\alpha}) p(\boldsymbol{\beta}) p(\boldsymbol{W})$$

where $p(\cdot)$ represents the probability of an event, $\boldsymbol{\alpha}$, $\boldsymbol{\beta}$ and $\boldsymbol{W}$ are hyperparameters in the GP kernel function and above problem can be solved equivalently by minimizing $-\ln p(\boldsymbol{X}, \boldsymbol{\alpha}, \boldsymbol{\beta}|\boldsymbol{\Theta})$ through a gradient descending algorithm. A similar approach in [38] is taken for initialization of latent variable $\boldsymbol{x}$ in model estimation. One attractive feature is that the periodic characteristic of the locomotion would allow use of the GPDM dynamics to estimate high-dimensional joint angles effectively and efficiently and therefore, it is feasible for real-time applications.

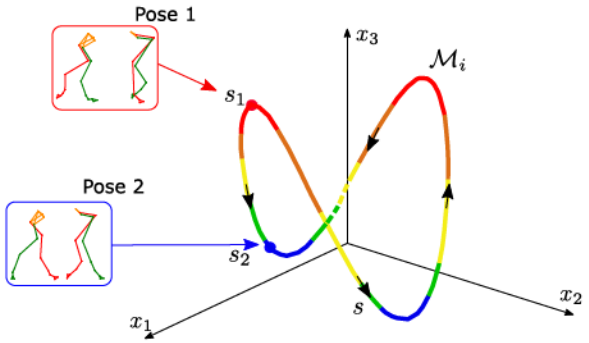

Fig. 6. Schematic of the learned latent manifolds and dynamics for pose estimation.

Unlike many reported GPDM applications, the model in (1) is parameterized by the gait phase variable s, namely, latent variable is given as $\boldsymbol{x}(s)$. The advantage of using s, rather than time variable t, is to capture the gait progression precisely and therefore, predict the joint angle $\boldsymbol{\theta}$. This treatment is attractive for estimation of all joint angles collectively and accurately. Fig. 6 illustrates the latent manifold $\mathcal{M}_i$ for pose estimation. The phase variable s and gait activity are obtained through an LSTM-based network with the similar structure as the classifier discussed in the previous section; see Fig. 4. We first train this network offline using the IMU measurement as input sequence with labeled data by the motion capture system. With the trained LSTM model, the IMU measurements are embedded to the high-dimensional joint angels through the phase variable. Due to the fast computation for the LSTM-based gait detection and low-dimensional GPDM implementation, the prediction can be achieved for real-time pose estimation.

V. Evaluation Metrics

In this section, we describe a few evaluation metrics for the lameness detection and pose estimation design.

A. Lameness Detection Metrics

Following metrics for lameness detection are used.

1) Detection Accuracy: Confusion matrix is used to capture and demonstrate the detection results. Confusion matrix is a table which summarizes the predictive results by listing the true label and predicted label of the testing data. Each row of the matrix represents the instances in a predicted class, while each column represents the instances in an actual class (or vice versa). In a binary classification with test data labeled as positive or negative (although the actual label can be defined in different ways in specific context), the confusion matrix is of the dimension 2 by 2. Particularly, the

four entries are named as True Positive (TP), True Negative (TN), False Positive (FP) and False Negative (FN). "Positive" means correctly prediction, while "false" refers to incorrect prediction.

Given the confusion matrix of each layer, we define several metrics to evaluate the performance of the classifiers, including recall and precision as

$$R_i = \frac{\mathrm{TP}_i}{\mathrm{TP}_i + \mathrm{FN}_i}, \quad P_i = \frac{\mathrm{TP}_i}{\mathrm{TP}_i + \mathrm{FP}_i} \tag{2}$$

and the accuracy is

$$\gamma_i = \frac{\mathrm{TP}_i + \mathrm{TN}_i}{\mathrm{TP}_i + \mathrm{FP}_i + \mathrm{TN}_i + \mathrm{FN}_i}, \tag{3}$$

where subscripts i = GC, LDW, LDT, LLW, LLT represent these classifiers of the three MLC layers. In calculating the accuracy, we exclude the incorrectly labeled data by previous layer. For instance, when calculating the accuracy for LDW, the input might include the trot data (incorrectly labeled as walk).

Given the above accuracy calculation for each classifier among three layers, the overall accuracy is obtained as

$$\gamma = \gamma_{\mathrm{GC}}\Big\{\alpha_{\mathrm{W}}\gamma_{\mathrm{LDW}}\big[\alpha_{\mathrm{NW}} + (1-\alpha_{\mathrm{NW}})\gamma_{\mathrm{LLW}}\big] + (1-\alpha_{\mathrm{W}})\gamma_{\mathrm{LDT}}\big[\alpha_{\mathrm{NT}} + (1-\alpha_{\mathrm{NT}})\gamma_{\mathrm{LLT}}\big]\Big\}, \tag{4}$$

where α_{W} denotes the portion of walk samples in the test pool, and α_{NW} and α_{NT} are the portions of normal walk and trot samples within walk and trot instances, respectively. The rationale for (4) is that a testing instance can be correctly labeled at γ_{GC} level, while such randomly chosen walk or trot instance is an intrinsic property of the test pool. One correctly labeled instance has the probability of α_{W} being further classified by lameness detection within walk or $(1-\alpha_{\mathrm{W}})$ within trot.

2) F-Measure: For multi-class classification, we also use F-Measure as a metric to assess the performance. F-Measure is a harmonic mean of recall and precision of the classifier

$$F_j = \frac{(\beta^2+1)P_j R_j}{\beta^2 P_j + R_j}, \quad j = \text{Micro, Macro}, \tag{5}$$

where β is the weight and P_{Micro} and R_{Micro} are defined as

$$P_{\mathrm{Micro}} = \sum_{i=1}^{n} P_i, \quad R_{\mathrm{Micro}} = \sum_{i=1}^{n} R_i$$

and $P_{\mathrm{Macro}} = \frac{1}{n}P_{\mathrm{Micro}}$ and $R_{\mathrm{Macro}} = \frac{1}{n}R_{\mathrm{Micro}}$, where P_i and R_i is precision and recall for the ith classifier that is defined in (2), and $n = 5$ is the total number of classifiers. The value of F-measure is ranged from zero to one, and high values of F-measure indicate preferable performance [45].

B. Pose Estimation Metrics

To quantify the accuracy of the joint angle estimation, several performance metrics are taken. The first metric is the mean and standard variation of the estimated joint angle errors that are calculated by using the motion capture system as the ground truth.

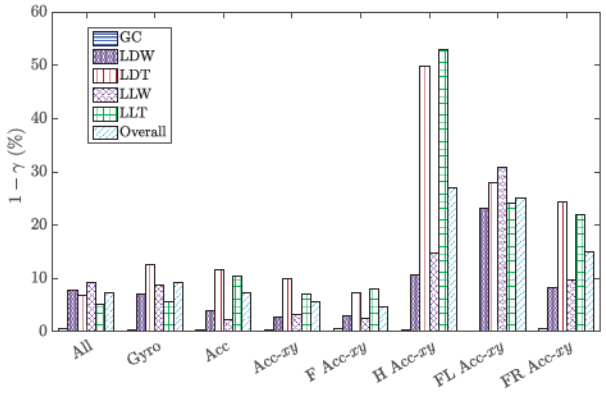

Fig. 7. Lameness detection accuracy for various combinations of selective IMU measurements. For the x-axis label, "All": all four IMU gyroscope and accelerometer measurements; "Gyro" ("Acc"): gyroscope (accelerometer) measurements from all four IMUs; "Acc-xy": accelerometer measurements in the xy (sagittal) plane; "F" ("H"): frontlimb (hindlimb); "FL" ("FR"): left (right) frontlimb. The axis labels are combination of these abbreviations. For instance, FL Acc-xy indicates that the xy channels of the accelerometer measurements in the front left limb IMU are used in the LSTM classifier.

Similar to [15] we evaluate the variability of joint angle θ within the multiple gait cycles by using the variance ratio VR_θ as

$$\mathrm{VR}_\theta = \frac{\sum_{i=1}^{N_s}\sum_{j=1}^{N_c}\left(\theta_{ij} - \bar{\theta}_i\right)^2 / N_s(N_c-1)}{\sum_{i=1}^{N_s}\sum_{j=1}^{N_c}\left(\theta_{ij} - \bar{\theta}\right)^2 / (N_c N_s - 1)} \tag{6}$$

where N_s is the number of samples in each gait cycle and N_c is the number of used gait cycles, θ_{ij} is the jth joint angle value at the ith sample point and $\bar{\theta}_i$ is the average ith joint angles over N_c cycles, $\bar{\theta}$ is the mean of the average joint angles, that is, $\bar{\theta} = \frac{1}{N_s}\sum_{i=1}^{N_s}\bar{\theta}_i$. The smaller VR value, the greater similarity (or repeatability) of each cycle of the gait.

We also use the intra-individual variability (IAV) and inter-individual variability (IEV) for capturing limb gait cycle-to-cycle variations among N_h horses as [46]

$$\mathrm{IAV}_\theta = \frac{1}{2N_h}\sum_{i=1}^{N_h}\left[\bar{\sigma}^{\,L}(\theta_i) + \bar{\sigma}^{\,R}(\theta_i)\right], \quad \mathrm{IEV}_\theta = \overline{\sigma}(\bar{\theta}),$$

where $\bar{\sigma}(\theta_i)$ is the average of the standard deviation of joint angle θ_i of the ith horse (over the N_c cycles), and superscripts "L" and "R" represent the left and right limbs, respectively. $\bar{\theta}$ in the above IEV_θ is the average of all N_h horses by using both the left and right limbs in N_c cycles. We will present these metrics results in the next section.

VI. Experimental Results

In this section, we present experimental results to illustrate the performance of the lameness detection and pose estimation design. The experimental data collected for this study include 16500 total strides (14000 outdoor + 2500 indoor). The data are randomly shuffled and then split into 80% and 20% for training and testing the machine learning methods. From these data, we obtain $\alpha_{\mathrm{W}} = 0.59$, $\alpha_{\mathrm{NW}} = 0.36$ and $\alpha_{\mathrm{NT}} = 0.37$ for parameters in (4). To build the GPDM model, $D = 24$ and $d = 4$ are used in implementation.

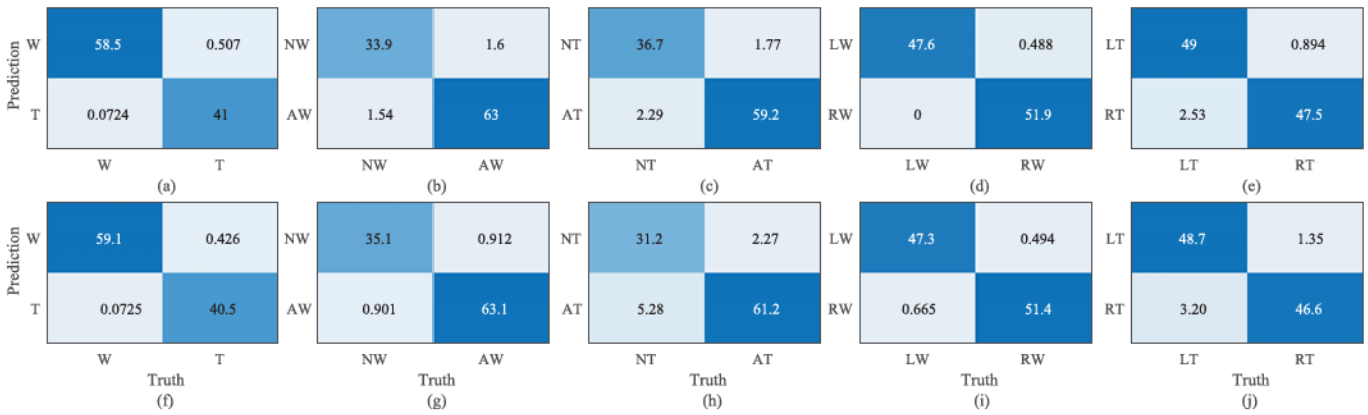

Fig. 8. Confusion matrix for RNN-LSTM (Top row) and Feature based (Bottom row) classifiers. (a) and (f) for GC layer, (b) and (g) for LDW, (c) and (h) for LDT, (d) and (i) for LLW, and (e) and (j) for LLT. Some other notations, W: walk, T: Trot, A: Abnormal, N: Normal, L: Left and R: Right.

TABLE II
LAMENESS DETECTION ACCURACY (%) COMPARISON

Classifier	GC	LDW	LDT	LLW	LLT	Overall
LSTM (F Acc-xy)	99.5	97.0	95.9	99.5	96.5	95.3
LSTM (All)	99.5	92.2	93.1	90.7	94.7	92.6
LSTM (All+withers)	99.6	94.1	90.8	93.5	94.8	92.7
Feature-based MLC	99.5	98.2	92.5	98.8	95.4	94.4
DCNN	–	–	–	–	–	93.6

A. Lameness Detection Results

For the feature-based MLC detection method, gyroscope and accelerometer measurements from all four wearable IMUs are used to form the gait feature matrix, while for the RNN-LSTM design, selective IMUs measurements are used. We first discuss how different selective combinations of the IMU data impact the lameness detection accuracy. Fig. 7 shows the lameness detection inaccuracy (i.e., $1-\gamma$) for all horses by using selective combinations of IMU measurements and IMU locations such as all limbs, forelimbs, or hindlimb. From these results, it is clear that the accuracy is more sensitive to accelerometer measurements than these of gyroscope. Moreover, the forelimb accelerometer measurements in the (xy) sagittal plane (labeled as "F Acc-xy" in the figure) are the most sensitive to detect the induced lameness. From this observation, for the RNN-LSTM design, we mainly present the detection results using such accelerometer measurements.

We now present the lameness detection results by the RNN-LSTM and the feature-based MLC methods. Fig. 8 shows confusion matrix results for each layer by these two methods. The top row in the figure shows the confusion matrices for each layer of the RNN-LSTM implementation and the bottom row for the feature-based MLC. It is clear that from these confusion matrices, the two methods demonstrate comparable results. Using (4), we compute the detection accuracy metrics for each layer. Table II lists the lameness detection accuracy at each layer. For the RNN-LSTM method, the overall accuracy by (4) is $\gamma_{\text{LSTM}} = 95.3\%$. For the feature-based MLC, the overall accuracy is calculated as $\gamma_{\text{MLC}} = 94.4\%$. The RNN-LSTM demonstrates a slightly better accuracy than that by the feature-based MLC. It is also interesting to notice that using all IMUs measurements or even with additional IMU at withers does not improve the lameness detection accuracy (with respectively only 92.6% and 92.7%). This might be due to different sensitivities of IMU signals for the induced gait changes.

We further compare the results with a deep concurrent neural network (DCNN) multi-class classifier [47]. A DCNN is formed by stacking three types of layers: convolutional layer, pooling layer, and fully connected layer. The training figures are constructed by applying DFT to the gait feature matrix and then take magnitude of each element [40]. Using the same training data and testing data, Fig. 9 shows corresponding confusion matrices by using feature-based MLC (Fig. 9(a)), DCNN (Fig. 9(b)), RNN-LSTM with all IMU signals (Fig. 9(c)) and RNN-LSTM with the forelimb accelerometer signals in the sagittal plane (Fig. 9(d)). Obviously, both feature-based MLC and RNN-LSTM (using the forelimb acceleration measurements in the xy-plane) have slightly higher accuracy rates than the DCNN. Using a radar chart, Fig. 10 further shows the classifier performance metrics ($\beta = 1$) defined in the previous section such as F_{Micro}, F_{Macro}, γ, etc. The RNN-LSTM (with "F Acc-xy") has the largest values in terms of each criterion than those under the feature-based MLC, which outperforms the DCNN and the RNN-LSTM with all IMUs.

B. Gait Estimation Results

Similar to the lameness detection results, we first compare how the selective IMU signals would impact on the joint angle estimation. Fig. 11 shows the average joint angle estimation errors for each limb by using various combinations of IMU signals. From these results, we observe that using the z-axial gyroscope measurements from four limb IMUs generates the comparable accuracy as using all IMUs (accelerometers and gyroscopes) measurements. One reason for such results might be due to that the z-axial angular rate measurements capture the joint angle motion in the sagittal plane. Therefore, in the following discussion, we only present the joint angle estimation by using the gyroscope z-axis (denoted as "gyro-z") measurements.

Fig. 12 shows the joint angle estimation for one normal walk and trot trial on treadmill by one horse. Similar to [17], we here present the estimation results of the relative joint

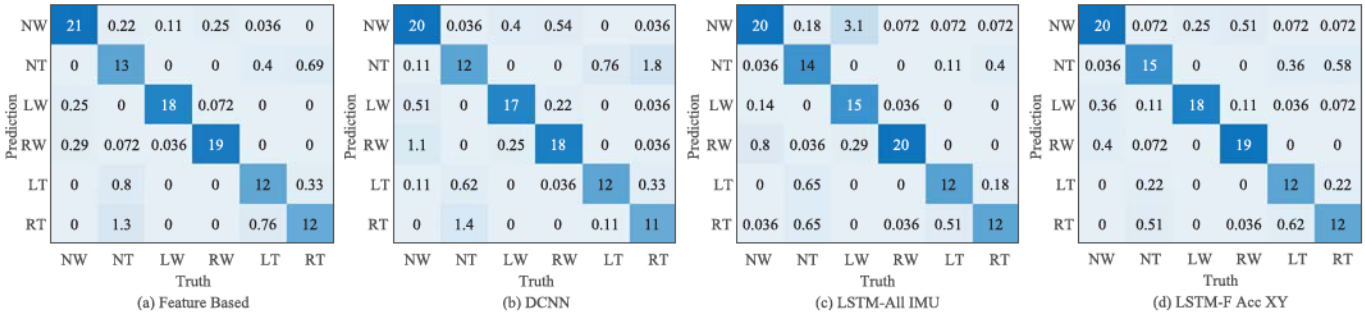

Fig. 9. Comparison of lameness classification results under the feature-based classifier, DCNN and RNN-LSTM with complete or partial IMU measurements (in percentage with respect to the entire testing data).

TABLE III
LIMB JOINT ANGLE ESTIMATION DIFFERENCES BETWEEN NORMAL AND ABNORMAL CONDITIONS UNDER WALK AND TROT

Gait	Forelimb (deg)					Hindlimb (deg)				
	θ^{F}_{Shd}	θ^{F}_{Elb}	θ^{F}_{Car}	θ^{F}_{Fet}	θ^{F}_{Cof}	θ^{H}_{Hip}	θ^{H}_{Stf}	θ^{H}_{Tar}	θ^{H}_{Fet}	θ^{H}_{Cof}
Walk	2.80 ± 1.4	8.95 ± 7.2	10.82 ± 11.6	7.58 ± 4.3	$\mathbf{13.90 \pm 10.5}$	2.45 ± 1.9	5.18 ± 6.7	7.75 ± 7.5	7.75 ± 5.8	$\mathbf{13.61 \pm 10.9}$
Trot	4.53 ± 3.5	12.67 ± 9.8	$\mathbf{17.83 \pm 13.2}$	11.18 ± 7.5	$\mathbf{25.74 \pm 7.5}$	9.58 ± 7.2	14.45 ± 8.8	$\mathbf{19.89 \pm 13.9}$	$\mathbf{17.70 \pm 8.5}$	$\mathbf{26.68 \pm 14.5}$

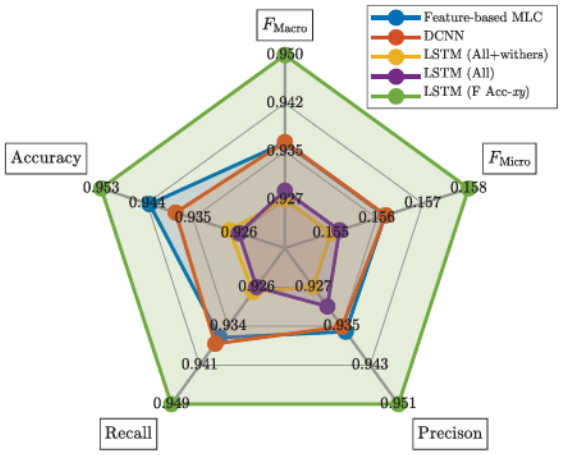

Fig. 10. Performance comparison of the multi-layer (RNN-LSTM and feature-based) and DCNN classifiers.

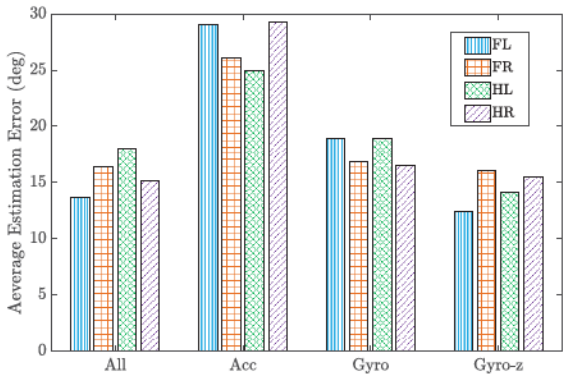

Fig. 11. Average joint angle prediction errors of each limb (4 strides) using various combinations of selective limb IMU measurements.

angles for each limb only. The estimated joint angles follow the ground truth for both walk and trot gaits. We also add the estimation for outdoor experiments in the figure and they are consistent with these on treadmill. Fig. 13 shows the calculation of all joint angle estimation errors for six horses for both walk and trot under normal and abnormal conditions (i.e., plastic shoes on). Figs. 13(a) and 13(c) show absolute errors and Figs. 13(b) and 13(d) for relative estimation errors for normal and abnormal gaits, respectively. The average estimation errors for all joint angles are less than 5 and 10 degs under normal and abnormal conditions, respectively, while the average relative errors are less than about 5% and 10%, respectively. Relatively large estimation errors and variations happen for the fetlock and coffin joints.

We take the fetlock joint angle comparison as an example to show joint angles difference between the normal and abnormal gaits. Fig. 14(a) shows the fetlock joint angle comparison for walk and Fig. 14(b) for trot. Plastic shoes were wore at the left forelimb in these experiments. It is clear that the fetlock joint angles show quite significant differences for both walk and trot. Table III further lists all joint angle estimation differences (mean and standard deviation) between the normal and abnormal conditions for walk and trot for all horses. We calculate the joint angle estimation differences for the forelimb and hindlimb by adding left and right limbs results in the table. For walk, coffin angles of both forelimb and hindlimb show significantly difference and for trot gait, carpus and coffin joints for forelimb and tarsus, fetlock and coffin joints for hindlimb are demonstrated significant difference. We further take a hypothesis test for difference between all 20 relative joint angles of four limbs under normal and abnormal conditions using t-test with 95% confidence. The results are shown significantly different for both walk and trot with $p_{\text{trot}} = 0.015$ and $p_{\text{walk}} = 0.024$.

To demonstrate the estimated joint angle variability and repeatability, we calculate the IAV and IEV defined in the previous section using the horse data on treadmill. Table IV lists the IAV and IEV for each joint angles of forelimb and hindlimb under normal and abnormal conditions for walk and trot. For normal trot, the IAV values for all joints and the IEV values for most joints are similar to those reported in [46] and

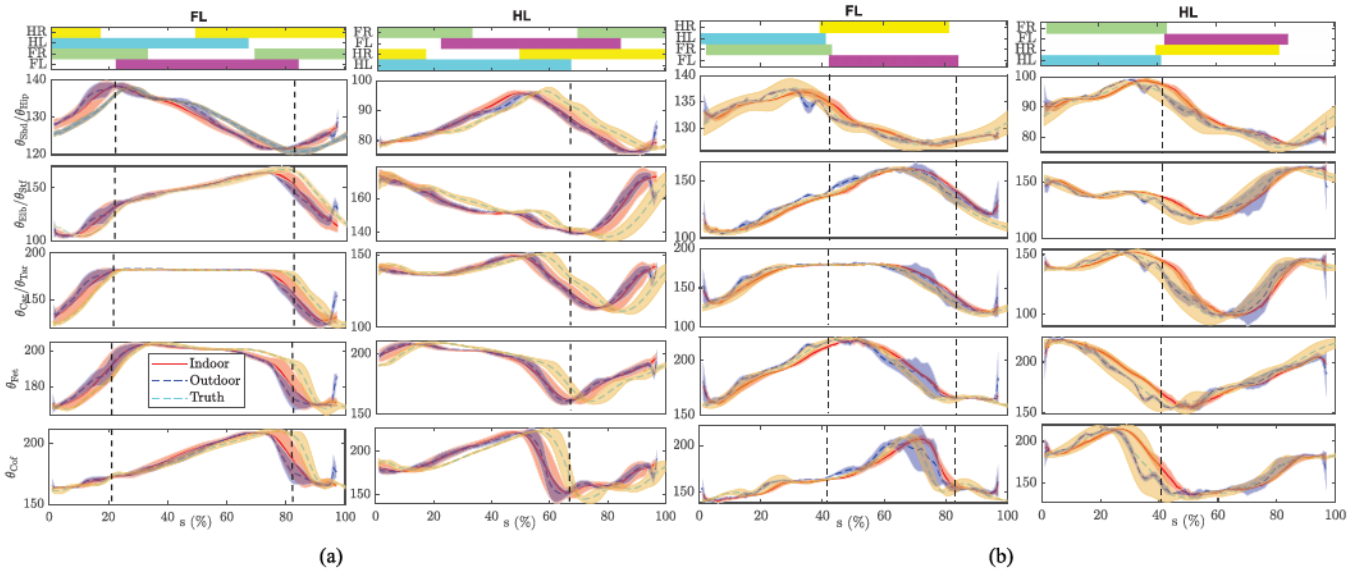

Fig. 12. Joint angle estimation (mean and standard deviation, in deg) of left forelimb (FL) and hindlimb (HL) for one horse (SN1) on treadmill. (a) Walk and (b) trot. The subfigures in each row shares the same label at y-axis.

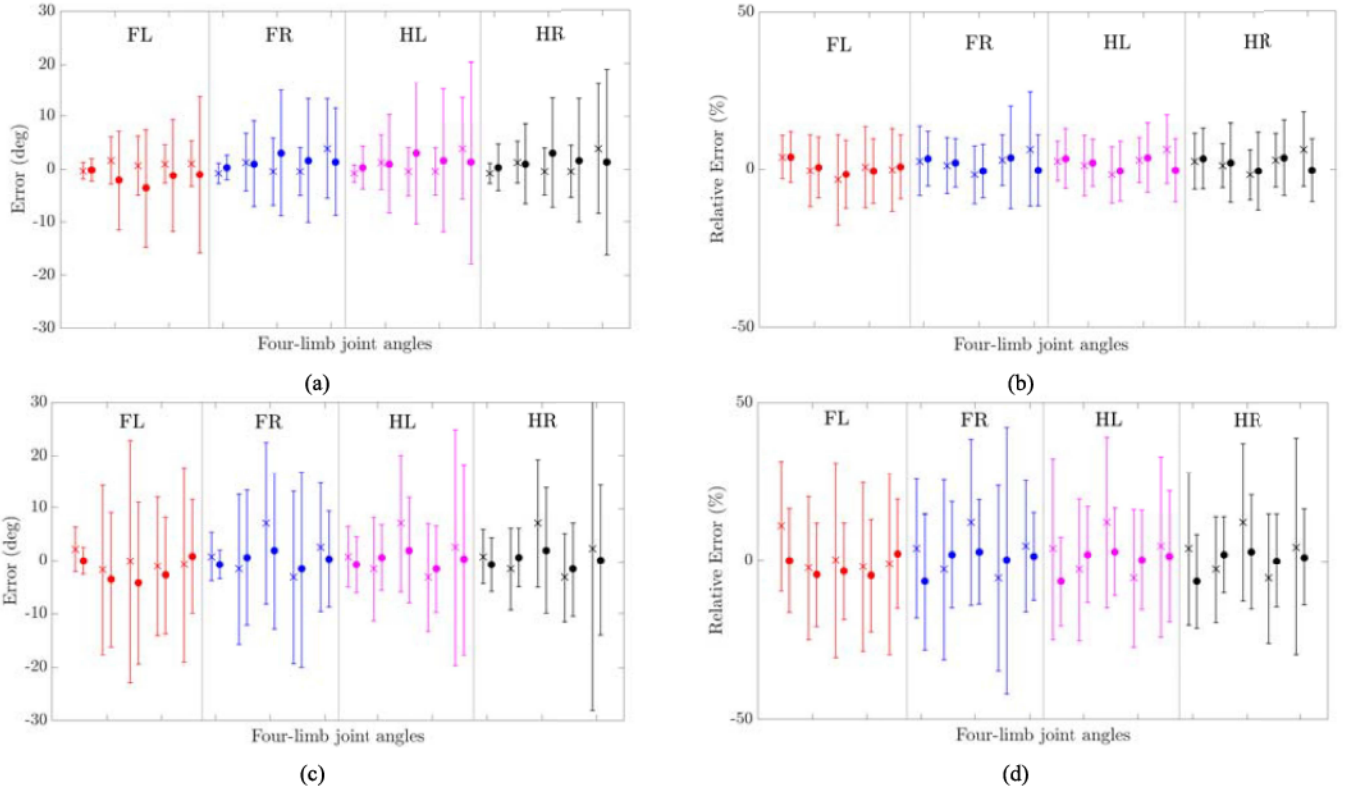

Fig. 13. Absolute and relative errors of the four-limb joint angle estimation for walk ("cross" markers) and trot ("circle" markers) for all horses on treadmill. For each of four limbs marked as "FL", "FR", "HL", and "HR", the plotted data follow the order of shoulder/hip, elbow/stifle, carpus/tarsus, fetlock, and coffin joint angles. (a) Absolute estimation errors under normal gaits. (b) Relative estimation errors under normal gaits. (c) Absolute estimation errors for abnormal gaits. (d) Relative estimation errors under abnormal gaits.

the IEV values for some hindlimb joints (tarsus, fetlock and coffin) are larger than the reported values. The IAV and IEV values for the walk gait are similar to or smaller than those for trot. Fig. 15 shows the calculated VR metric for all 20 joints for walk and trot gaits under normal and abnormal conditions using the estimated joint angles. For normal trot, the VR values demonstrate similar trends and ranges reported in [15], [16]. We also notice that most VR values for normal walk are slightly larger than those for normal trot. This is consistent with the reported results that reducing velocity would decrease the gait variability [48]. Furthermore, the VR values under abnormal conditions are in general larger than those under normal conditions for both walk and trot. This observation is also consistent with the IAV and IEV metrics.

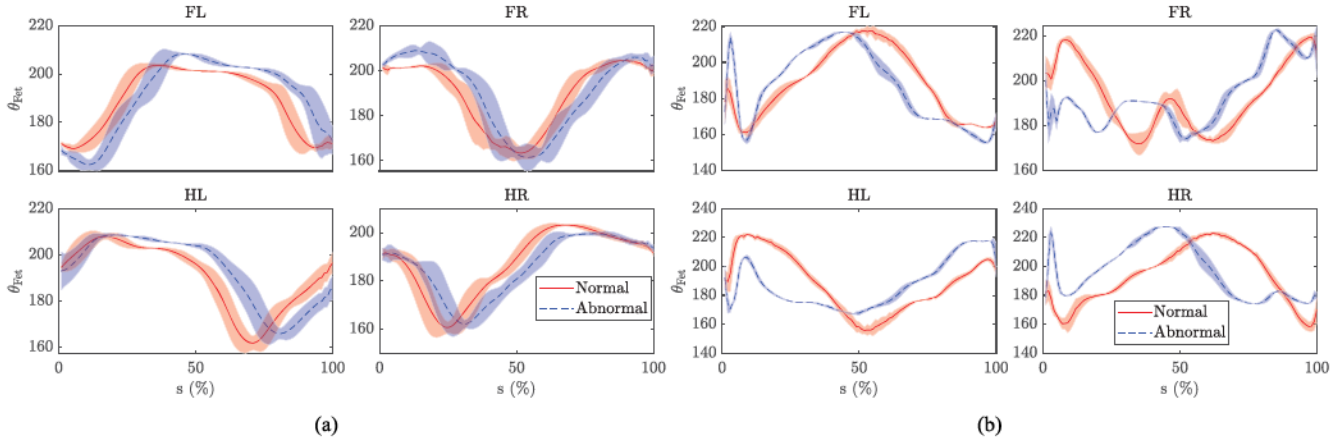

Fig. 14. Fetlock angle estimation θ_{Fet} (in deg) comparison for normal and abnormal conditions. (a) Walk and (b) trot gaits.

TABLE IV

IAV AND IEV FROM THE ESTIMATED JOINT ANGLES FOR ALL HORSES UNDER NORMAL AND ABNORMAL CONDITIONS FOR WALK AND TROT

Gait		Forelimb					Hindlimb				
		θ^F_{Shd}	θ^F_{Elb}	θ^F_{Car}	θ^F_{Fet}	θ^F_{Cof}	θ^H_{Hip}	θ^H_{Stf}	θ^H_{Tar}	θ^H_{Fet}	θ^H_{Cof}
Normal walk	IAV	1.44	4.75	4.21	3.00	5.17	1.52	3.40	3.94	4.26	8.38
	IEV	5.65	4.40	7.18	5.25	8.74	8.15	3.92	4.75	5.25	9.42
Abnormal walk	IAV	4.21	14.52	11.01	7.31	11.12	3.60	5.68	7.53	5.38	11.78
	IEV	6.40	15.76	12.34	10.94	13.13	7.27	5.61	9.13	6.67	12.49
Normal trot	IAV	1.29	3.19	3.19	3.96	5.44	1.74	3.21	4.46	4.51	6.50
	IEV	4.61	5.82	4.34	5.14	6.32	5.42	4.22	11.2	13.3	14.14
Abnormal trot	IAV	2.35	8.10	10.43	8.33	10.17	5.20	6.55	9.13	7.20	12.31
	IEV	6.54	11.15	10.39	9.00	12.34	9.62	13.40	9.31	10.32	14.65

VII. DISCUSSION

In the proposed multi-layer structure, each classifier is a binary classifier and Fig. 16 shows the precision and recall (PR) curve comparison of the gait classier, and lameness detection classifiers in walk and trot. The PR curves of the LSTM-based classifier performs similar to the DCNN classifier, maintaining almost 100% for all recall values, which outperform the classical feature-based classifier. To compare the performance with the existing wearable sensor-based approach, we follow the methods described in [49] to compute the maximum difference of withers (i.e., WDmax) between two consecutive peaks in a gait cycle. Since the change of WDmax is one of the indications for forelimb lameness, it is used for the lameness detection [49]. We set the mean and standard deviation of WDmax as 3.6 ± 12.5 mm for all normal gait cycles as a threshold to evaluate detection accuracy. Using the same data set, the calculation results in $\gamma_{\text{WDmax}} = 72\%$ of accuracy. Therefore, the proposed machine learning-based approaches in this study outperform the result by using asymmetric time-domain feature (i.e., WDmax).

The joint angle estimation is built on the learned latent manifolds (1) for each gait activity. Figs. 17(a) and 17(b) show the learned manifolds for walk and trot, respectively. The latent manifolds under both the normal and abnormal conditions are included in the figure. Both manifolds are 4-dimensional closed curves (the fourth dimension is shown by the colored value for each point). It is clear that manifolds are regular

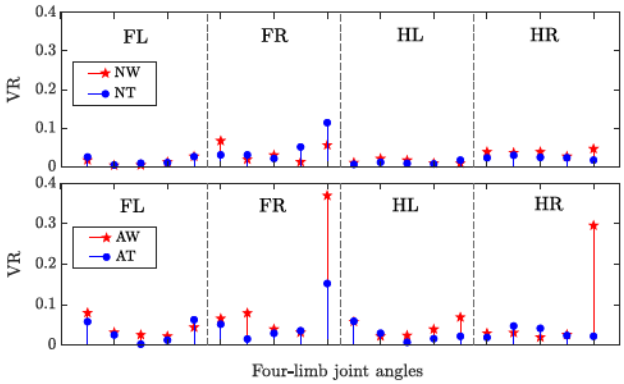

Fig. 15. Calculated VR values for all joints for walk and trot gaits under normal and abnormal conditions. The top plot shows the normal walk (NW) and normal trot (NT) and the bottom for abnormal walk (AW) and abnormal trot (AT).

closed curves because of periodic, symmetric motion for walk and trot. Under the abnormal condition, the manifold curves look close to these under normal walk or trot with small variations.

Using the symmetry property, it was reported in [24] to use a single IMU to estimate the lower-limb joint angles for human walk gaits. Therefore, it is of interests to understand whether a single limb IMU is capable to estimate all limb joint angles. Figs. 18(a) and 18(b) show the total estimation errors of left and right limbs for 10 joint angles of forelimb and hindlimb by using different gyroscope measurements for walk

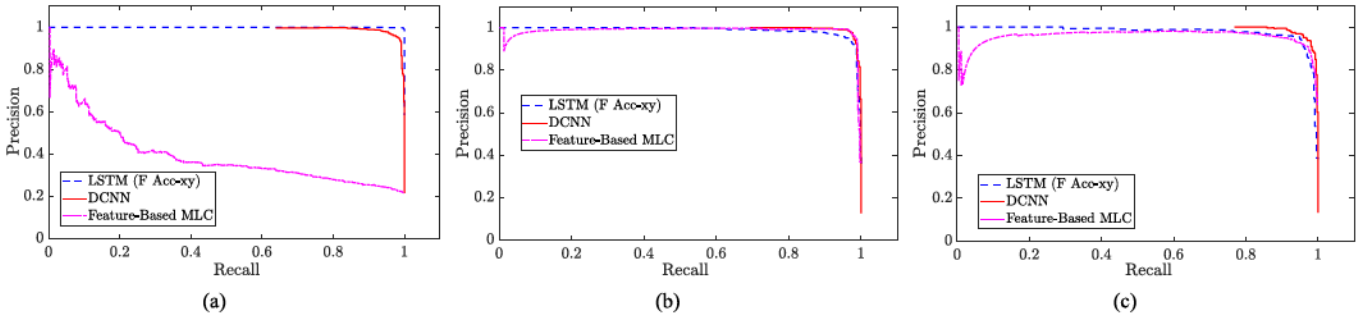

Fig. 16. PR curve comparison among various classification methods for (a) gait classification, lameness detection in (b) walk and (c) trot.

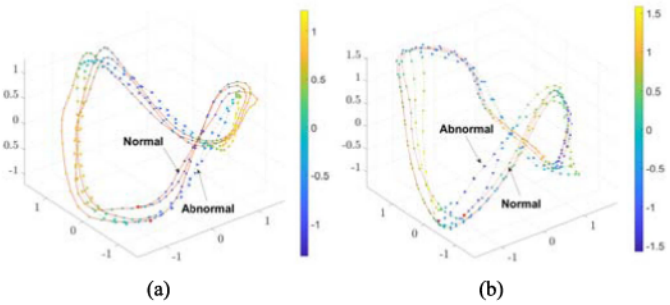

Fig. 17. Latent manifolds for (a) walk and (b) trot for normal and abnormal conditions.

under normal and abnormal conditions, respectively. Under the normal condition (Fig. 18(a)), the prediction errors by using four gyroscopes' z-axis component (labeled as "Gyro-z") are at the same level to these by using a single gyroscope on each limb (labeled as "FL/FR/HL/HR gyro-z"). Therefore, it is feasible to use one IMU to estimate all joint angles under normal gait condition. On the other hand, when a plastic shoe was on the left forelimb (Fig. 18(b)), only the estimation error using the gyroscope on the same limb has the similar level by using all gyroscopes. Using gyroscope measurements on other limbs (i.e., FR, HL or HR) however generates much larger errors. The main reason for large estimation errors is due to that the gyroscopes on other limbs cannot precisely capture the joint angles for the limb with plastic shoe. This result implies that when the lameness occurrence and location is unknown, four limb gyroscopes are necessary for obtaining accurate pose estimation.

Meanwhile, for lameness detection, we similarly try to reduce the number of the used wearable IMUs. Fig. 18(c) shows the lameness detection inaccuracy rates under using combinations of accelerometer measurements from different limb IMUs. The lameness was introduced on the left or the right forelimb. Detection inaccuracy rates of the three layers (GC, LDW, LDT) and overall lameness detection are plotted under four combination cases: using the left or right forelimb IMU accelerometer to detect the case when a plastic shoe was on left or right forelimb. When the IMU accelerometer on the limb with the shoe was selected and used for detection (i.e., FL-L and FR-R), the lameness detection accuracy is high (over 90%). However, when the IMU accelerometer on the other limb (i.e., FL-R and FR-L) was used for detection, the accuracy rate dropped significantly (overall rates dropped below 80% and 40%, respectively). We also tried to use the IMU accelerometers attached on hindlimb and the accuracy rates dropped even further. Those results imply that four limb IMUs are necessary if lameness or abnormal gait might occur to any limb. It is also of interests to notice from Fig. 18(c) that the gait classification (GC) accuracy by using any combinations of the IMU accelerometer data is over 99% and this implies that the walk and trot gaits are easily classified even with one IMU attached on any of four limbs.

The outdoor experiments were conducted on the unpaved dirt road with small pebbles and the indoor experiments on the treadmill. We consider the influence of terrain conditions on joint angle estimation. Fig. 19 shows the joint angle estimation errors (mean and one standard deviation) for walk gait in indoor and outdoor experiments. The estimation errors for indoor experiments are calculated as the difference with the ground truth, while for outdoor experiments as the difference with the indoor estimates because of no ground truth in outdoor experiments. The mean and standard deviation values maintain at the similar levels for all joint angles in indoor and outdoor experiments. Because its proximity to terrain surface, we further consider the hoof angle estimates and conduct hypotheses testings of the differences between any two data sets of the indoor ground truth, and the estimates in indoor and outdoor experiments. The testing results show no significant differences at the 95% confidence level and the p-value is 0.98. The plausible explanations for these comparison results include: (1) the difference of the terrain conditions is not significant to cause any pose changes for trot or walk gaits, and (2) the IMU measurements do not capture the pose change given a limited number of the sensors used. Further experiments are needed to test the influence of terrain conditions on the pose estimation scheme.

Given low-cost of video cameras and fast growing computational capability, the vision-based method has been used for animal lameness detection, e.g., [50], [51]. Comparing with the vision-based lameness detection, the wearable IMU-based approach has several advantages. First, one single camera only obtains a partial view of the horse motion. To obtain all limb motion data, multiple cameras are needed to place around a horse and imaging acquisition and processing have to be synchronized among cameras. Second, the wearable IMU measurements provide more sensitive and accurate gait event detection such as toe touch-down and heel lift-off than vision-based methods, which is particularly attractive for equestrian

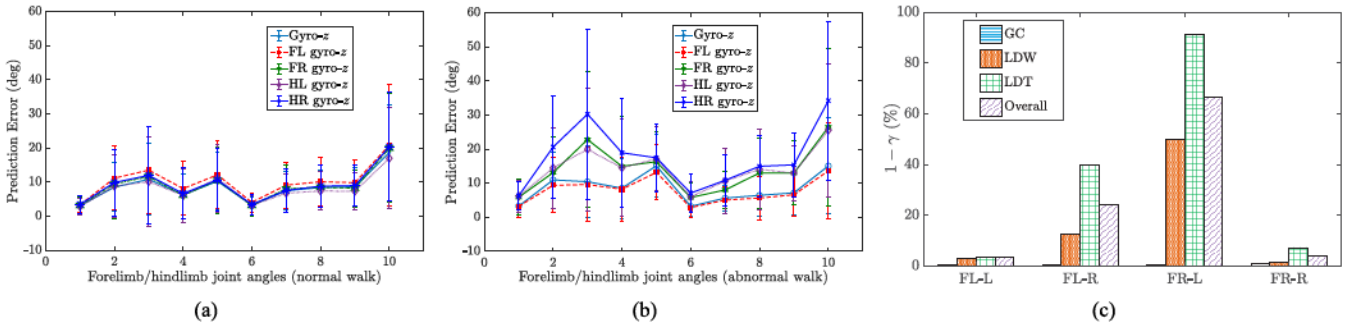

Fig. 18. Joint angle prediction errors under (a) normal and (b) abnormal conditions by various combination of the gyroscope measurements. The joint angles errors in the figure are calculated by taking the left and right limbs together. (c) Lameness detection accuracy under the LSTM design by using measurements from selective IMUs on different limbs. For the x-axis label and figure legends, "FL" ("FR"): left (right) frontlimb and "L" ("R"): induced lameness on left (right) frontlimb. The axis labels and legend are combination of the two abbreviations. For instance, "FL-R" indicates using the IMU measurements on the left forelimb to detect the induced lameness on the right forelimb. "FL gyro-z" represents using the z-axis component of the IMU gyroscope on the left forelimb to estimate all joint angles.

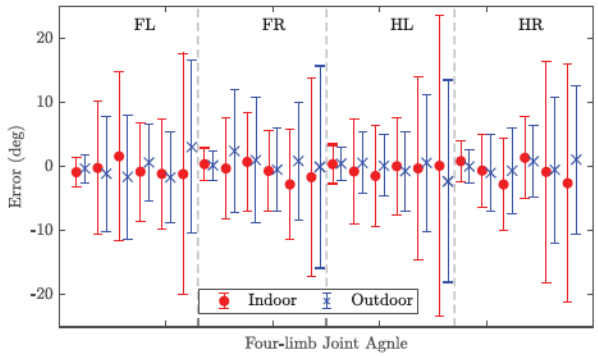

Fig. 19. Indoor and outdoor joint angle estimation errors (mean and standard deviation) for normal walk gait.

training on sandy ground. Finally, the IMU measurement data size is much smaller compared with the video/image data and therefore, the computational cost is low and can be used in outdoor farming field without the need of infrastructure setup to install ground cameras.

The induced horse lameness in this study was not from pathological conditions and indeed it was gait alterations. Lameness considered here represents a symptom of any deviation of the normal gait, namely, abnormal gait. This is consistent with recent discussion in [3]. Although the lameness detection and pose estimation design has been successfully demonstrated, this study has several limitations. First, the lameness detection and pose estimation results were primarily built on treadmill and limited outdoor experiments. In experiments, we only tried to put the plastic shoe on the forelimb to induce the lameness gaits. It is a limitation for not including experiments to introduce additional abnormal conditions on hindlimb or multiple shoes at the same time to comprehensively validate the detection and estimation approach. This study does not consider and address the accuracy issues from the motion capture markers that are attached on horse skin. The LSTM-based lameness detection and GPDM pose estimation methods have the attractive property for real-time applications but the presented results in this paper are not from real-time implementation. Finally, only walk and trot gaits are used as examples to test and validate the design and both gaits are symmetric locomotion. It is of interests to extend and apply the proposed lameness detection and pose estimation approach to other types of horse gaits, particularly asymmetric gaits.

VIII. Conclusion

We presented a learning-based multi-layer classifier for horse limb lameness detection and a limb pose estimation scheme for walk and trot. The lameness and gait activity detection scheme used indoor and outdoor motion data collected by a set of four wearable IMUs on limbs. The multi-layer classifier enabled to transfer the original multi-class classification problem into three independent binary classification sub-problems to recognize horse gaits, and step-by-step detect and identify lameness. Both the RNN-LSTM and the feature-based SVM/KNN algorithms were used to implement the multi-layer classifiers. The limb pose estimation was built on the learned motion latent manifolds with the detected gait activity. We tested the lameness detection and pose estimation design by extensive experiments under normal and induced lameness conditions. Both the RNN-LSTM and feature-based detection algorithms achieved more than 94% detection accuracy. The estimated joint angle errors were also less than 5 and 10 degs for under normal and abnormal conditions, respectively. Besides high accuracy and many other advantages by using wearable limb IMUs, the proposed RNN-LSTM lameness detection and the manifold learning-based pose estimation method is potentially capable for real-time applications.

Acknowledgment

The authors would like to thank Dr. Helio Manso of the Universidade Federal Rural de Pernambuco in Recife, Brazil, for his suggestions and support during data collection.

References

[1] *Feeding the World by Controlling Animal Diseases*, World Organization for Animal Health, Paris, France, 2018.

[2] P. R. van Weeren, T. Pfau, M. Rhodin, L. Roepstorff, F. S. Braganca, and M. A. Weishaupt, "Do we have to redefine lameness in the era of quantitative gait analysis," *Equine Veter. J.*, vol. 49, no. 5, pp. 567–569, 2017.

[3] S. Adair *et al.*, "Letter to the editor: A response to 'what is lameness and what (or who) is the gold standard to detect it,'" *Equine Veter. J.*, vol. 51, no. 2, pp. 270–272, 2019.

[4] *National Economic Cost of Equine Lameness, Colic, and Equine Protozoal Myeloencephalitis (EPM) in the United States*, United States Department of Agriculture, Animal and Plant Health Inspection Service, Fort Collins, CO, USA, Oct. 2001.

[5] *Science Breakthroughs to Advance Food and Agricultural Research by 2030*, National Academies of Sciences, Engineering, and Medicine, National Academies Press, Washington, DC, USA, 2019.

[6] J. B. A. Loomans, P. W. T. Stolk, P. R. van Weeren, H. Vaarkamp, and A. Barneveld, "A survey of the workload and clinical skills in current equine practices in The Netherlands," *Equine Veterinary Educ.*, vol. 19, no. 3, pp. 162–168, Apr. 2007.

[7] T. Pfau, A. Fiske-Jackson, and M. Rhodin, "Quantitative assessment of gait parameters in horses: Useful for aiding clinical decision making?" *Equine Veterinary Educ.*, vol. 28, no. 4, pp. 209–215, Apr. 2016.

[8] K. G. Keegan *et al.*, "Repeatability of subjective evaluation of lameness in horses," *Equine Veterinary J.*, vol. 42, no. 2, pp. 92–97, Feb. 2010.

[9] S. Egan, P. Brama, and D. McGrath, "Research trends in equine movement analysis, future opportunities and potential barriers in the digital age: A scoping review from 1978 to 2018," *Equine Veterinary J.*, vol. 51, no. 6, pp. 813–824, Nov. 2019.

[10] R. P. Bell *et al.*, "Associations of force plate and body-mounted inertial sensor measurements for identification of hind limb lameness in horses," *Amer. J. Veterinary Res.*, vol. 77, no. 4, pp. 337–345, Apr. 2016.

[11] E. Olsen, P. H. Andersen, and T. Pfau, "Accuracy and precision of equine gait event detection during walking with limb and trunk mounted inertial sensors," *Sensors*, vol. 12, no. 6, pp. 8145–8156, Jun. 2012.

[12] J.-N. Lee, M.-W. Lee, Y.-H. Byeon, W.-S. Lee, and K.-C. Kwak, "Classification of horse gaits using FCM-based neuro-fuzzy classifier from the transformed data information of inertial sensor," *Sensors*, vol. 16, no. 5, p. 664, May 2016.

[13] J. Haladjian, J. Haug, S. Nüske, and B. Bruegge, "A wearable sensor system for lameness detection in dairy cattle," *Multimodal Technol. Interact.*, vol. 2, no. 2, p. 27, May 2018.

[14] I. Halachmi, M. Guarino, J. Bewley, and M. Pastell, "Smart animal agriculture: Application of real-time sensors to improve animal well-being and production," *Annu. Rev. Animal Biosci.*, vol. 7, no. 1, pp. 403–425, Feb. 2019.

[15] W. Back *et al.*, "How the horse moves: 1. Significance of graphical representations of equine forelimb kinematics," *Equine Veterinary J.*, vol. 27, no. 1, pp. 31–38, Jan. 1995.

[16] W. Back *et al.*, "How the horse moves: 2. Significance of graphical representations of equine hind limb kinematics," *Equine Veterinary J.*, vol. 27, no. 1, pp. 39–45, Jan. 1995.

[17] E. Hodson, H. M. Clayton, and J. L. Lanovaz, "The forelimb in walking horses: 1. Kinematics and ground reaction forces," *Equine Veterinary J.*, vol. 32, no. 4, pp. 287–294, Jul. 2000.

[18] E. Hodson, H. M. Clayton, and J. L. Lanovaz, "The hindlimb in walking horses: 1. Kinematics and ground reaction forces," *Equine Veterinary J.*, vol. 33, no. 1, pp. 38–43, Jan. 2001.

[19] J. Figueiredo, P. Felix, L. Costa, J. C. Moreno, and C. P. Santos, "Gait event detection in controlled and real-life situations: Repeated measures from healthy subjects," *IEEE Trans. Neural Syst. Rehabil. Eng.*, vol. 26, no. 10, pp. 1945–1956, Oct. 2018.

[20] Z. Wang *et al.*, "Inertial sensor-based analysis of equestrian sports between beginner and professional riders under different horse gaits," *IEEE Trans. Instrum. Meas.*, vol. 67, no. 11, pp. 2692–2704, Nov. 2018.

[21] Y. Huang *et al.*, "Real-time intended knee joint motion prediction by deep-recurrent neural networks," *IEEE Sensors J.*, vol. 19, no. 23, pp. 11503–11509, Dec. 2019.

[22] A. S. Alharthi, S. U. Yunas, and K. B. Ozanyan, "Deep learning for monitoring of human gait: A review," *IEEE Sensors J.*, vol. 19, no. 21, pp. 9575–9591, Nov. 2019.

[23] M. Trkov, K. Chen, J. Yi, and T. Liu, "Inertial sensor-based slip detection in human walking," *IEEE Trans. Automat. Sci. Eng.*, vol. 17, no. 1, pp. 348–360, Jul. 2019.

[24] S. Chen, S. S. Bangaru, T. Yigit, M. Trkov, C. Wang, and J. Yi, "Real-time walking gait estimation for construction workers using a single wearable inertial measurement unit (IMU)," in *Proc. IEEE/ASME Int. Conf. Adv. Intell. Mechatronics (AIM)*, Jul. 2021, pp. 753–758.

[25] K. G. Keegan *et al.*, "Assessment of repeatability of a wireless, inertial sensor-based lameness evaluation system for horses," *Amer. J. Veterinary Res.*, vol. 72, no. 9, pp. 1156–1163, Sep. 2011.

[26] J. F. Marshall, D. G. Lund, and L. C. Voute, "Use of a wireless, inertial sensor-based system to objectively evaluate flexion tests in the horse," *Equine Veterinary J.*, vol. 44, pp. 8–11, Dec. 2012.

[27] T. Pfau *et al.*, "Head, withers and pelvic movement asymmetry and their relative timing in trot in racing thoroughbreds in training," *Equine Veterinary J.*, vol. 50, no. 1, pp. 117–124, Jan. 2018.

[28] M. J. McCracken *et al.*, "Comparison of an inertial sensor system of lameness quantification with subjective lameness evaluation," *Equine Veterinary J.*, vol. 44, no. 6, pp. 652–656, Nov. 2012.

[29] K. G. Keegan *et al.*, "Comparison of a body-mounted inertial sensor system-based method with subjective evaluation for detection of lameness in horses," *Amer. J. Veter. Res.*, vol. 74, no. 1, pp. 17–24, 2013.

[30] Y. Huang, M. Kaufmann, E. Aksan, M. J. Black, O. Hilliges, and G. Pons-Moll, "Deep inertial poser: Learning to reconstruct human pose from sparse inertial measurements in real time," *ACM Trans. Graph.*, vol. 37, no. 6, pp. 1–15, Dec. 2018.

[31] G. P. Panebianco, M. C. Bisi, R. Stagni, and S. Fantozzi, "Analysis of the performance of 17 algorithms from a systematic review: Influence of sensor position, analysed variable and computational approach in gait timing estimation from IMU measurements," *Gait Post.*, vol. 66, pp. 76–82, Oct. 2018.

[32] J. Cao, W. Li, C. Ma, and Z. Tao, "Optimizing multi-sensor deployment via ensemble pruning for wearable activity recognition," *Inf. Fusion*, vol. 41, pp. 68–79, May 2018.

[33] M. Hildebrand, "The quadrupedal gaits of vertebrates," *BioScience*, vol. 39, no. 11, pp. 766–775, Dec. 1989.

[34] J. J. Robilliard, T. Pfau, and A. M. Wilson, "Gait characterisation and classification in horses," *J. Experim. Biol.*, vol. 210, no. 2, pp. 187–197, Jan. 2007.

[35] D. Warner, E. Vasseur, D. M. Lefebvre, and R. Lacroix, "A machine learning based decision aid for lameness in dairy herds using farm-based records," *Comput. Electr. Agric.*, vol. 169, pp. 1–7, Feb. 2020.

[36] J. Kaler, J. Mitsch, J. A. Vázquez-Diosdado, N. Bollard, T. Dottorini, and K. A. Ellis, "Automated detection of lameness in sheep using machine learning approaches: Novel insights into behavioural differences among lame and non-lame sheep," *Royal Soc. Open Sci.*, vol. 7, no. 1, pp. 1–13, 2019.

[37] F. M. S. Bragança *et al.*, "Improving gait classification in horses by using inertial measurement unit (IMU) generated data and machine learning," *Sci. Rep.*, vol. 10, no. 1, Dec. 2020, Art. no. 17785.

[38] K. Chen, Y. Zhang, J. Yi, and T. Liu, "An integrated physical-learning model of physical human-robot interactions with application to pose estimation in bikebot riding," *Int. J. Robot. Res.*, vol. 35, no. 12, pp. 1459–1476, 2016.

[39] T. Yigit, F. Han, E. Rankins, J. Yi, K. McKeever, and K. Malinowski, "Wearable IMU-based early limb lameness detection for horses using multi-layer classifiers," in *Proc. IEEE 16th Int. Conf. Autom. Sci. Eng. (CASE)*, Aug. 2020, pp. 956–961.

[40] W. Jiang and Z. Yin, "Human activity recognition using wearable sensors by deep convolutional neural networks," in *Proc. 23rd ACM Int. Conf. Multimedia*, Oct. 2015, pp. 1307–1310.

[41] W. Back, W. Hartman, H. C. Schamhardt, G. Bruin, and A. Barneveld, "Kinematic response to a 70 day training period in trotting Dutch warmbloods," *Equine Veterinary J.*, vol. 27, no. S18, pp. 127–131, Jun. 2010.

[42] *Noraxon USA, Ultium EMG*. Accessed: Mar. 10, 2020. [Online]. Available: https://www.noraxon.com/our-products/ultium-emg/

[43] J. E. Shroyer, "Kinematic analysis of the collected and extended jog and lope of the stock breed western pleasure horse," Ph.D. dissertation, Dept. Animal Sci. Kinesiol., Auburn Univ., Auburn, AL, USA, 2010.

[44] S. Hochreiter and J. Schmidhuber, "Long short-term memory," *Neural Comput.*, vol. 9, no. 8, pp. 1735–1780, 1997.

[45] D. M. Powers, "Evaluation: From precision, recall and F-measure to ROC, informedness, markedness and correlation," *J. Mach. Learn. Technol.*, vol. 2, no. 1, pp. 37–63, 2011.

[46] C. Degueurce, P. Pourcelot, F. Audigié, J. M. Denoix, and D. Geiger, "Variability of the limb joint patterns of sound horses at trot," *Equine Veterinary J.*, vol. 29, no. S23, pp. 89–92, May 1997.

[47] A. Ren *et al.*, "SC-DCNN: Highly-scalable deep convolutional neural network using stochastic computing," *ACM SIGPLAN Notices*, vol. 52, no. 4, pp. 405–418, 2016.

[48] A. M. Cruz, B. Vidondo, A. A. Ramseyer, and U. E. Maninchedda, "Effect of trotting speed on kinematic variables measured by use of extremity-mounted inertial measurement units in nonlame horses performing controlled treadmill exercise," *Amer. J. Veterinary Res.*, vol. 79, no. 2, pp. 211–218, Feb. 2018.

[49] T. Pfau, M. F. S. Caviedes, R. McCarthy, L. Cheetham, B. Forbes, and M. Rhodin, "Comparison of visual lameness scores to gait asymmetry in racing thoroughbreds during trot in-hand," *Equine Veterinary Educ.*, vol. 32, no. 4, pp. 191–198, Apr. 2020.

[50] X. Kang, X. D. Zhang, and G. Liu, "A review: Development of computer vision-based lameness detection for dairy cows and discussion of the practical applications," *Sensors*, vol. 21, no. 3, pp. 1–26, 2021.

[51] J. Gardenier, J. Underwood, and C. Clark, "Object detection for cattle gait tracking," in *Proc. IEEE Int. Conf. Robot. Autom. (ICRA)*, May 2018, pp. 2206–2213.

Tarik Yigit (Graduate Student Member, IEEE) received the B.S. degree in mechanical engineering from Middle East Technical University, Ankara, Turkey, in 2012. He is currently pursuing the Ph.D. degree in mechanical engineering with Rutgers University, NJ, USA.

He attended the Turkish Military Academy, Ankara, in 2012, as a Research Assistant. His research interests include physical human–robot interaction (HRI), bipedal and quadruped biomechanics, dynamic systems and control, robotics, and machine learning with particular focus on HRI.

Feng Han (Graduate Student Member, IEEE) received the B.S. degree in aerospace engineering from the Nanjing University of Aeronautics and Astronautics, Nanjing, China, in 2017, and the M.S. degree in aerospace engineering from the Harbin Institute of Technology, Harbin, China, in 2019. He is currently pursuing the Ph.D. degree in mechanical and aerospace engineering with Rutgers University, NJ, USA.

His research interests include dynamics, control, and machine learning with the applications to robotics.

Ellen Rankins received the B.S. degree from Auburn University in 2016 and the M.S. degree from the University of Florida in 2018. She is currently pursuing the Ph.D. degree with the Endocrinology and Animal Biosciences Graduate Program.

Her research interests include equine biomechanics, behavior, and applied physiology with applications in equine assisted services and the human–horse interaction. Her scholarly pursuits have been supported through many scholarships and fellowships, including the P.E.O. Scholar Award, the Rutgers University School of Environmental and Biological Sciences Excellence Fellowship, the Phi Kappa Phi National Fellowship, and the Spirit of Auburn Scholarship. She has served as the Graduate Student Representative for the Equine Science Society from 2019 to 2021.

Jingang Yi (Senior Member, IEEE) received the B.S. degree in electrical engineering from Zhejiang University, Hangzhou, China, in 1993, the M.Eng. degree in precision instruments from Tsinghua University, Beijing, China, in 1996, and the M.A. degree in mathematics and the Ph.D. degree in mechanical engineering from the University of California, Berkeley, CA, USA, in 2001 and 2002, respectively.

He is currently a Professor of Mechanical Engineering at Rutgers University. His research interests include autonomous robotic systems, dynamic systems and control, mechatronics, and automation science and engineering, with applications to biomedical systems, civil infrastructure, and transportation systems. He is a fellow of the American Society of Mechanical Engineers (ASME). He was a recipient of the 2010 U.S. NSF CAREER Award. He has served as an Associate Editor for IEEE TRANSACTIONS ON AUTOMATION SCIENCE AND ENGINEERING, IEEE/ASME TRANSACTIONS ON MECHATRONICS, IEEE ROBOTICS AND AUTOMATION LETTERS, *IFAC Journal on Mechatronics*, *Control Engineering Practice*, and *Journal of Dynamic Systems, Measurement, and Control* (ASME). He serves as a Senior Editor for the IEEE ROBOTICS AND AUTOMATION LETTERS and IEEE TRANSACTIONS ON AUTOMATION SCIENCE AND ENGINEERING. He serves as an Associate Editor for the *International Journal of Intelligent Robotics and Applications*.

Kenneth H. McKeever received the B.S. degree in animal science from California State Polytechnic University in 1979, the M.S. degree in animal science from Fresno State University in 1981, and the Ph.D. degree in animal physiology from The University of Arizona in 1984.

From 1985 to 1987, he has worked for two years as the National Academies of Sciences-National Research Council Resident Research Associate at the Cardiovascular Research Laboratory, NASA Ames Research Center, CA, USA. From 1987 to 1994, he has developed and coordinated research at the Equine Exercise Physiology Laboratory, Ohio State University. Since 1995, he has been with the Department of Animal Sciences, Rutgers University, where he is currently a Professor and serves as the Associate Director for the Rutgers University Equine Science Center. He has published more than 220 book chapters, journal articles and proceedings papers, and more than 70 abstracts that have advanced our understanding of the athletic horse. His research interests include comparative exercise and cardiovascular physiology and the effects of performance enhancing practices on the physiological responses of the equine athlete. He is the Scientist (first) to be named a fellow of the American College Sports Medicine for work with horses and he is the first and only Equine Physiologist named a fellow by the American Physiological Society. He serves as the President for the Equine Science Society as well as the Editor-in-Chief for the journal *Comparative Exercise Physiology*.

Karyn Malinowski received the B.S. and M.S. degrees in animal science and the Ph.D. degree in zoology from Rutgers University, New Brunswick, NJ, USA, in 1978, 1980, and 1986, respectively.

Since 1978, she has been working as a Faculty Member with the School of Environmental and Biological Sciences, Rutgers University, in various roles, including as an Extension Specialist in Equine Sciences, an Animal Sciences Professor, the Founding Director of the Equine Science Center, and the Director of the Rutgers Cooperative Extension. She is currently a Professor of Animal Science and the Founding Director of the Rutgers Equine Science Center, New Jersey Agricultural Experiment Station (NJAES). She has played a lead role in building the equine science program at Rutgers University and in the formation of the Rutgers Equine Science Center. Her research interests include improving the well-being and quality of life of the equine athlete while ensuring the vitality and viability of the equine industry, both statewide and nationally.